

Polarizability of nanowires at surfaces: Exact solution for general geometry

Jesper Jung* and Thomas G. Pedersen

Department of Physics and Nanotechnology, Aalborg University, Skjernvej 4A, DK-9220
Aalborg Øst, Denmark and Interdisciplinary Nanoscience Center (iNANO), Denmark

[*jung@nano.aau.dk](mailto:jung@nano.aau.dk)

Abstract: The polarizability of a nanostructure is an important parameter that determines the optical properties. An exact semi-analytical solution of the electrostatic polarizability of a general geometry consisting of two segments forming a cylinder that can be arbitrarily buried in a substrate is derived using bipolar coordinates, cosine-, and sine-transformations. Based on the presented expressions, we analyze the polarizability of several metal nanowire geometries that are important within plasmonics. Our results provide physical insight into the interplay between the multiple resonances found in the polarizability of metal nanowires at surfaces.

© 2018 Optical Society of America

OCIS codes: (000.3860) Mathematical methods in physics; (240.6680) Surface plasmons; (230.5750) Resonators.

References and links

1. S. A. Maier, *Plasmonics: Fundamentals and Applications* (Springer, 2007).
2. L. Novotny and B. Hecht, *Principles of Nano-optics* (Cambridge 2006).
3. A. V. Zayats and I. I. Smolyaninov, "Near-field photonics: surface plasmon polaritons and localized surface plasmons," *J. Opt. A: Pure Appl. Opt.* **5**, S16-S50 (2003).
4. S. A. Maier and H. A. Atwater, "Plasmonics: Localization and guiding of electromagnetic energy in metal/dielectric structures," *J. Appl. Phys.* **98**, 011101 (2005).
5. W. A. Murray and W. L. Barnes, "Plasmonic materials," *Adv. Mater.* **19**, 3771–3782 (2007).
6. S. Lal, S. Link, and N. J. Halas, "Nano-optics from sensing to waveguiding," *Nat. Photon.* **1**, 641–648 (2007).
7. M. Moskovits, "Surface-enhanced spectroscopy," *Rev. Mod. Phys.* **57**, 783–826 (1985).
8. Y. C. Coa, R. Jin, and C. A. Mirkin, "Nanoparticles with Raman spectroscopic fingerprints for DNA and RNA detection," *Science* **297**, 1536–1540 (2002).
9. A. J. Haes and R. P. V. Duyne, "A nanoscale optical biosensor: sensitivity and selectivity of an approach based on the localized surface plasmon resonance spectroscopy of triangular silver nanoparticles," *J. Am. Chem. Soc.* **124**, 10596–10604 (2002).
10. K. R. Catchpole and A. Polman, "Plasmonic solar cells," *Opt. Express* **16**, 21793–21800 (2008).
11. H. A. Atwater and A. Polman, "Plasmonics for improved photovoltaic devices," *Nat. Mater.* **9**, 205–213 (2010).
12. V. E. Ferry, J. N. Munday, and H. A. Atwater, "Design considerations for plasmonic photovoltaics," *Adv. Mater.* **22**, 4794–4808 (2010).
13. L. Lorenz, "Lysbevægelsen i og udenfor en af plane lysbølger belyst kugle," *K. Dan. Vidensk. Selsk. Skr.* **6**, 1–62 (1890).
14. G. Mie, "Beitrage zur optik trüber medien speziell kolloidaler metallosungen," *Ann. Physik.* **330**, 337–445 (1908).
15. C. F. Bohren and D. R. Huffman, *Absorption and Scattering of Light by Small Particles* (Wiley, 1983).
16. L. Rayleigh, "The dispersal of light by a dielectric cylinder," *Phil. Mag.* **36**, 365–376 (1918).
17. J. R. Wait, "Scattering of a plane wave from a circular cylinder at oblique incidence," *Can. J. Phys.* **33**, 189–195 (1955).
18. A. Taflove and S. Hagness, *Computational Electrodynamics: The Finite-Difference Time-Domain Method* (Artech House, 2000).
19. J. Jin, *The Finite Element Method in Electrodynamics* (Wiley, 2002).

20. T. Søndergaard, "Modeling of plasmonic nanostructures: Green's function integral equation methods," *Phys. Status Solidi B* **244**, 3448–3462 (2007).
21. O. J. F. Martin, C. Girard, and A. Dereux, "Generalized field propagator for electromagnetic scattering and light confinement," *Phys. Rev. Lett.* **74**, 526–529 (1995).
22. F. J. Garcia de Abajo and A. Howie, "Retarded field calculation of electron energy loss in inhomogenous dielectrics," *Phys. Rev. B* **65**, 115418 (2002).
23. J. Jung, T. G. Pedersen, T. Søndergaard, K. Pedersen, A. N. Larsen and B. B. Nielsen, "Electrostatic plasmon resonances of metal nanospheres in layered geometries," *Phys. Rev. B* **81**, 125413 (2010).
24. F. Hallermann, C. Rockstuhl, S. Fahr, G. Seifert, S. Wackerow, H. Graener, G. V. Plessen, and F. Lederer, "On the use of localized plasmon polaritons in solar cells," *Phys. Status Solidi (a)* **205**, 2844–2861 (2008).
25. J. W. Yoon, W. J. Park, K. J. Lee, S. H. Song, and R. Magnusson, "Surface-plasmon mediated total absorption of light into silicon," *Opt. Express* **19**, 20673–20680 (2011).
26. P. C. Waterman, "Surface fields and the T matrix," *J. Opt. Soc. Am. A* **16**, 2968–2977 (1999).
27. A. V. Radchik, A. V. Paley, G. B. Smith, and A. V. Vagov, "Polarization and resonant absorption in intersecting cylinders and spheres," *J. Appl. Phys.* **76**, 4827–4835 (1994).
28. A. Salandrino, A. Alu, and N. Engheta, "Parallel, series, and intermediate interconnects of optical nanocircuit elements. I. Analytical solution," *J. Opt. Soc. Am. B* **24**, 3007–3013 (2007).
29. M Pitkonen, "A closed-form solution for the polarizability of a dielectric double half-cylinder," *J. Electromagn. Waves Appl.* **24**, 1267–1277 (2010).
30. H. Kettunen, H. Wallen, and A. Sihvola, "Polarizability of a dielectric hemisphere," *J. Appl. Phys.* **102**, 044105 (2007).
31. Y. Luo, J. B. Pendry, and A. Aubry, "Surface plasmons and singularities," *Nano Lett.* **10**, 4186–4191 (2010).
32. Y. Luo, A. Aubry, and J. B. Pendry, "Electromagnetic contribution to surface-enhanced Raman scattering from rough metal surfaces: A transformation optics approach," *Phys. Rev. B* **83**, 155422 (2011).
33. J. Jung and T. G. Pedersen, "Exact polarizability and plasmon resonances of partly buried nanowires," *Opt. Express* **19**, 22775–22785 (2011).
34. P. M. Morse and H. Feshbach, *Methods of Theoretical Physics, Part II* (McGraw-Hill Book Company Inc., 1953).
35. H. E. Lockwood, *A Book of Curves* (Cambridge University Press, 1963).
36. A. Jonquiere "Note sur la serie $\sum_{n=1}^{\infty} \frac{x^n}{n^2}$," *Bulletin de la Socit Mathematique de France*, **17**, 142–152 (1889).
37. P. B. Johnson and R. W. Christy, "Optical constants of the noble metals," *Phys. Rev. B* **6**, 4370–4379 (1972).
38. J. R. Arias-Gonzalez and M. Nieto-Vesperinas, "Resonant near-field eigenmodes of nanocylinders on flat surfaces under both homogenous and inhomogenous lightwave excitation," *J. Opt. Soc. Am. A* **18**, 657–665 (2001).
39. A. Aubry, D. Y. Lei, S. A. Maier, and J. B. Pendry, "Plasmonic hybridization between nanowires and a metallic surface: A transformation optics approach," *ACS Nano* **5** 3293–3308 (2011).

1. Introduction

The electric polarizability of a nanoparticle, i.e. the relative tendency of the electron cloud to be distorted from its normal shape by an external field, is an important concept because it determines the particle's optical properties. Given the polarizability, it is usually straightforward to determine the light scattering and absorption properties of a nanoparticle [1, 2]. By illuminating a *metal* nanoparticle, collective excitations of the free conduction electrons of the metal can be resonantly excited. Such excitations are known as *particle plasmons* or *localized surface plasmons* [3–6] and give rise to resonances in the polarizability. Thus, given the polarizability of a metal nanoparticle, its particle plasmons can easily be identified. Particle plasmon resonances are interesting from an application point of view because they allow for strong light scattering and large electromagnetic fields in the vicinity of the particles. These properties suggest a variety of applications, e.g. within surface enhanced raman scattering [7], biomedical detection [8, 9], and plasmon enhanced solar cells [10–12]. Spherical nanoparticles can be analyzed analytically using the old, but famous Lorenz-Mie scattering theory [13–15] and, also, the "two-dimensional" case of a small cylinder has been analyzed a long time ago [16, 17]. However, for more complicated structures, no analytical solutions can in general be found. In the analysis of such structures, sophisticated numerical schemes such as finite difference time domain [18], finite element [19], or Green's function integral equation [20–23] approaches are often utilized. However, such approaches are complicated and from a computational point of view often very time-consuming. Thus, analytical modeling, whenever possible, is always favorable.

In the present paper, we present a semi-analytical analysis of the polarizability of the very general geometry shown in Fig. 1(a). The geometry is two-dimensional in the sense that it is

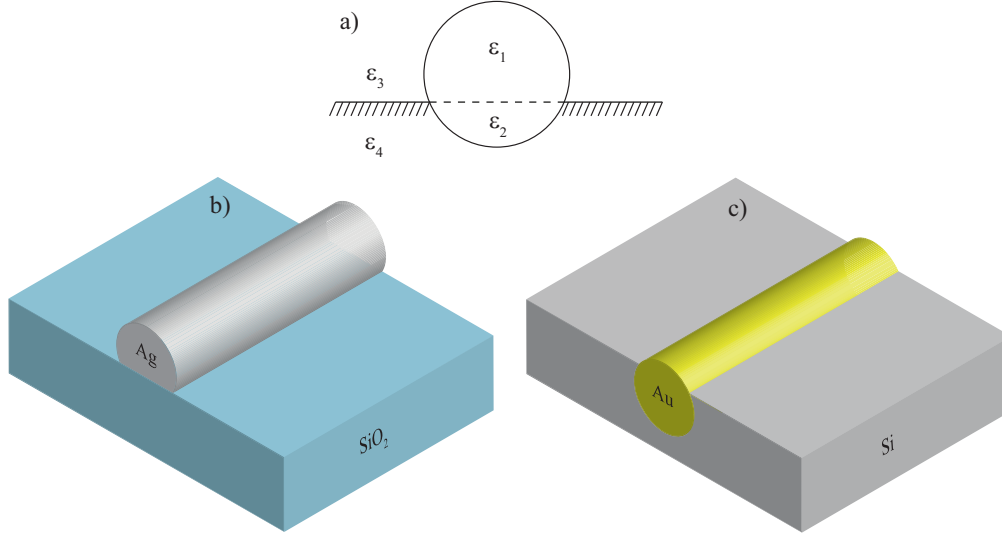


Fig. 1. (a) cross section of the geometry under consideration. The optical properties are described by the four dielectric constants ϵ_1 to ϵ_4 . (b) and (c) two examples of geometries that can be analyzed using the approach.

invariant under translation along the direction out of the paper. It consists of two domains, described by the dielectric constants ϵ_1 and ϵ_2 , which together form a cylinder. This cylinder may be placed in a background composed of two semi-infinite half-spaces with optical properties described by the dielectric constants ϵ_3 and ϵ_4 . As the interface can cut the cylinder at an arbitrary position and all four dielectric constants can be chosen freely, the structure allows for the study of several different geometries. Two examples are depicted in Fig. 1(b) and (c). In (b), we have chosen $\epsilon_1 = \epsilon_{\text{Ag}}$, $\epsilon_2 = \epsilon_4 = \epsilon_{\text{SiO}_2}$, and $\epsilon_3 = \epsilon_{\text{air}}$, whereas in (c), we have chosen $\epsilon_1 = \epsilon_2 = \epsilon_{\text{Au}}$, $\epsilon_4 = \epsilon_{\text{Si}}$, and $\epsilon_3 = \epsilon_{\text{air}}$. Both configurations are interesting in connection with plasmon assisted solar cells, see e.g. Refs. [24, 25]. Previously, simpler geometries such as half cylinders [26] or double half-cylinders in *homogenous* surroundings have been analyzed [27–29]. Also, a double half-sphere consisting of two conjoint hemispheres with different dielectric constants has been analyzed [30]. Recently convex and concave rough metal surfaces formed by cylindrical protrusions have been studied by Pendry and coworkers using the approach of transformation optics (TO) [31, 32]. They analyzed cut cylindrical protrusions on semi-infinite metal surfaces. This is opposite to the present work, where we only consider dielectric surfaces. In fact, the present approach cannot be used to analyze metal surfaces because we are interested in the polarizability which will lose its well defined meaning for a metal nanowire on an infinite metal surface. However, the TO approach of Refs. [31, 32] is also restricted in the sense that the dielectric constant of the protrusion and the surface must be identical. Thus, by carefully comparing the TO approach to the present it can be seen that they are in fact capable of analyzing complimentary structures. The present paper is a significant extension of our previous work, presented in Ref. [33], where we analyzed the polarizability of two conjoint half-cylinders embedded in two semi-infinite half spaces. Compared to Ref. [33], the present approach is much more general in that we allow for an arbitrary degree of burial of the nanowire. The approach of Ref. [33] is restricted to half-buried nanowires only. As a consequence the new scheme is

better suited for representing realistic experimental geometries. It can, e.g., handle nanowires with very different aspect ratios, i.e. wires with very different height/width ratios, and it can handle arbitrary contact angles between a nanowire and the supporting substrate. Furthermore, the present work provides more physical insight into the different resonances that come into play when the polarizability of complicated metal nanostructures are considered.

The paper is organized as follows. In Sec. 2, we present a derivation of the electrostatic polarizability of the geometry sketched in Fig. 1(a). Section 3 presents calculations and an analysis of the polarizability and its resonances for several important geometries. In Sec. 4, we offer our conclusions.

2. Theory

A detailed schematic of the geometry studied is shown in Fig. 2. It consists of four regions 1, 2, 3, and 4. A cylinder of radius r is cut by an infinite interface at an arbitrary position d from its center $|d| \leq r$. The segment of the cylinder above (below) the interface is denoted 1 (2) and has optical properties described by ϵ_1 (ϵ_2). The surrounding medium above (below) the interface is denoted 3 (4) and has a dielectric constant ϵ_3 (ϵ_4). To comply with the symmetry of the problem

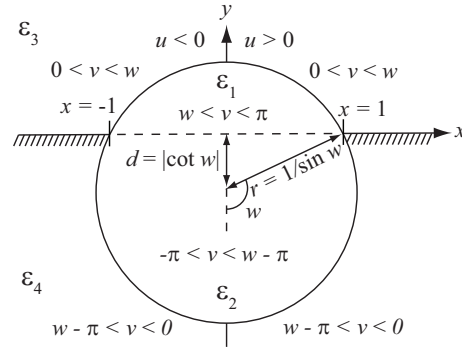


Fig. 2. Cross section of the geometry analyzed. In bipolar coordinates (u and v), the four different regions in the xy plane are given as $\epsilon_1 : \{-\infty < u < \infty \text{ and } w < v < \pi\}$, $\epsilon_2 : \{-\infty < u < \infty \text{ and } -\pi < v < w - \pi\}$, $\epsilon_3 : \{-\infty < u < \infty \text{ and } 0 < v < w\}$, and $\epsilon_4 : \{-\infty < u < \infty \text{ and } w - \pi < v < 0\}$.

it is an advantage to switch to the bipolar coordinates u and v defined as [34, 35]

$$x = \frac{\sinh u}{\cosh u - \cos v} \quad \text{and} \quad y = \frac{\sin v}{\cosh u - \cos v}. \quad (1)$$

The domains of u and v for the four different regions are shown in Fig. 2. The cut of the interface can be expressed in terms of the angle w , which we, with no loss of generality, choose between $0 < w < \pi$. The surface of the cylinder is defined such that $v = w$ on the part above the interface and $v = w - \pi$ on the part below the interface. In terms of w , the radius of the cylinder is given as $r = 1/\sin w$ and the distance from the center of the cylinder to the interface is given as $d = |\cot w|$. It should be noted that the geometry is defined such that the distance unit is half the intersection of the nanowire by the substrate plane, i.e. half the dashed line in Fig. 2. When investigating a geometry with a specific physical dimension the polarizabilities obtained in the present work should therefore be multiplied by the square of this distance measured in physical units in order to convert the results into standard units.

The analysis is started by assuming that all four dielectric constants are linear, isotropic, homogeneous, and frequency dependent and that the nanowire diameter is small compared to the wavelength (e.g. < 50 nm at optical wavelengths). The latter allows us to perform an electrostatic analysis. We therefore introduce the electrostatic potential $\phi(\mathbf{r})$ which is related to the electrostatic electric field as $\mathbf{E}(\mathbf{r}) = -\nabla\phi(\mathbf{r})$. The electrostatic potential must fulfil Laplace's equation

$$\nabla^2\phi(\mathbf{r}) = 0 \quad \forall \mathbf{r}, \quad (2)$$

with boundary conditions $\phi_i = \phi_j$ and $\varepsilon_i \hat{n} \cdot \nabla\phi_i = \varepsilon_j \hat{n} \cdot \nabla\phi_j$ on S , where the subscripts i and j refer to the different domains (1,2,3, and 4) and S to the boundaries. In order to derive the polarizability we first set up expressions for the electrostatic potential and its normal derivative in each of the four regions and then match these using the boundary conditions above.

The total potential $\phi_i(u, v)$ is written as a sum of the incident potential $\phi_0(u, v)$ and the scattered potential $\bar{\phi}_i(u, v)$. We consider the two linear independent polarizations along y and x , vertical and horizontal, respectively. For vertical (horizontal) polarization we look for solutions that are even (odd) functions of x and thereby u . Thus, for vertical polarization we may write the potential using cosine-transformations as

$$\phi_i(u, v) = \int_0^\infty \bar{\phi}_i(\lambda, v) \cos(\lambda u) d\lambda, \quad \bar{\phi}_i(\lambda, v) = \frac{2}{\pi} \int_0^\infty \phi_i(u, v) \cos(\lambda u) du, \quad (3)$$

and for horizontal polarization we may write using sine-transformations

$$\phi_i(u, v) = \int_0^\infty \bar{\phi}_i(\lambda, v) \sin(\lambda u) d\lambda, \quad \bar{\phi}_i(\lambda, v) = \frac{2}{\pi} \int_0^\infty \phi_i(u, v) \sin(\lambda u) du. \quad (4)$$

In order to comply with the Laplace equation, the scattered part of the potential in λ, v coordinates may be written as

$$\bar{\phi}_i(\lambda, v) = c_i(\lambda) \cosh(\lambda v) + s_i(\lambda) \sinh(\lambda v). \quad (5)$$

For vertical and horizontal polarizations the incident potentials are given as

$$\phi_0^{(v)}(u, v) = -\frac{\sin v}{\cosh u - \cos v} \begin{cases} 1 & \text{for } v > 0 \\ \frac{\varepsilon_3}{\varepsilon_4} & \text{for } v < 0 \end{cases} \quad \text{and} \quad \phi_0^{(h)}(u, v) = -\frac{\sinh u}{\cosh u - \cos v}, \quad (6)$$

respectively. Utilizing the approach presented in Ref. [33], it is easy to show that the vertical and horizontal polarizabilities may be found as

$$\alpha^{(v)} = 4\pi \int_0^\infty \lambda s_3(\lambda) d\lambda \quad \text{and} \quad \alpha^{(h)} = 4\pi \int_0^\infty \lambda c_3(\lambda) d\lambda. \quad (7)$$

The constants $s_3(\lambda)$ and $c_3(\lambda)$ can be derived using the boundary conditions. In order to utilize the boundary conditions for the normal derivative of the potential, we need the following two expressions for the derivative with respect to v of the incident potential. By taking the derivative of Eq. (6) and using Eqs. (3) and (4) it can be shown that

$$\frac{\partial}{\partial v} \bar{\phi}_0^{(v)}(\lambda, v) = \frac{2\lambda \cosh[\lambda(\pi - |v|)]}{\sinh[\lambda\pi]} \quad \text{and} \quad \frac{\partial}{\partial v} \bar{\phi}_0^{(h)}(\lambda, v) = \frac{2\lambda \sinh[\lambda(\pi - |v|)]}{\sinh(\lambda\pi)} \text{sgn}(v). \quad (8)$$

With the notation $C_{pq} \equiv \cosh[\lambda(p\pi - qw)]$ and $S_{pq} \equiv \sinh[\lambda(p\pi - qw)]$ the continuity of the potential for both polarizations yields

$$\begin{aligned} c_1(\lambda)C_{01} - s_1(\lambda)S_{01} &= c_3(\lambda)C_{01} - s_3(\lambda)S_{01}, \\ c_2(\lambda)C_{11} - s_2(\lambda)S_{11} &= c_4(\lambda)C_{11} - s_4(\lambda)S_{11}, \\ c_1(\lambda)C_{10} + s_1(\lambda)S_{10} &= c_2(\lambda)C_{10} - s_2(\lambda)S_{10}, \\ c_3(\lambda) &= c_4(\lambda). \end{aligned} \quad (9)$$

For vertical polarization the boundary conditions for the normal derivative of the potential yields

$$\begin{aligned}
\varepsilon_1 \left[-c_1(\lambda)S_{01} + s_1(\lambda)C_{01} + \frac{2C_{11}}{S_{10}} \right] &= \varepsilon_3 \left[-c_3(\lambda)S_{01} + s_3(\lambda)C_{01} + \frac{2C_{11}}{S_{10}} \right], \\
\varepsilon_2 \left[-c_2(\lambda)S_{11} + s_2(\lambda)C_{11} + \frac{\varepsilon_3}{\varepsilon_4} \frac{2C_{01}}{S_{10}} \right] &= \varepsilon_4 \left[-c_4(\lambda)S_{11} + s_4(\lambda)C_{11} + \frac{\varepsilon_3}{\varepsilon_4} \frac{2C_{01}}{S_{10}} \right], \\
\varepsilon_1 \left[c_1(\lambda)S_{10} + s_1(\lambda)C_{10} + \frac{2}{S_{10}} \right] &= \varepsilon_2 \left[-c_2(\lambda)S_{10} + s_2(\lambda)C_{10} + \frac{\varepsilon_3}{\varepsilon_4} \frac{2}{S_{10}} \right], \\
\varepsilon_3 s_3(\lambda) &= \varepsilon_4 s_4(\lambda),
\end{aligned} \tag{10}$$

and for horizontal polarization they read

$$\begin{aligned}
\varepsilon_1 \left[-c_1(\lambda)S_{01} + s_1(\lambda)C_{01} + \frac{2S_{11}}{S_{10}} \right] &= \varepsilon_3 \left[-c_3(\lambda)S_{01} + s_3(\lambda)C_{01} + \frac{2S_{11}}{S_{10}} \right], \\
\varepsilon_2 \left[-c_2(\lambda)S_{11} + s_2(\lambda)C_{11} + \frac{2S_{01}}{S_{10}} \right] &= \varepsilon_4 \left[-c_4(\lambda)S_{11} + s_4(\lambda)C_{11} + \frac{2S_{01}}{S_{10}} \right], \\
\varepsilon_1 [c_1(\lambda)S_{10} + s_1(\lambda)C_{10}] &= \varepsilon_2 [-c_2(\lambda)S_{10} + s_2(\lambda)C_{10}], \\
\varepsilon_3 s_3(\lambda) &= \varepsilon_4 s_4(\lambda).
\end{aligned} \tag{11}$$

By solving the equation system formed by the 8 equations of Eqs. (9) and (10) [Eqs. (9) and (11)], $s_3(\lambda)$ [$c_3(\lambda)$] can be found and the polarizability can be calculated using Eq. (7). Generally both the solution of $s_3(\lambda)$ and $c_3(\lambda)$ are fractions on the form $2N/(DS_{10})$, where D and N are given as

$$D = \sum_{p,q} D_{pq} C_{pq} \quad \text{and} \quad N = \sum_{p,q} N_{pq} \{C_{pq} - C_{10}\} \tag{12}$$

with

$$\begin{aligned}
D_{20} &= (\varepsilon_1 + \varepsilon_2)(\varepsilon_1 + \varepsilon_3)(\varepsilon_2 + \varepsilon_4)(\varepsilon_3 + \varepsilon_4), \\
D_{24} &= (\varepsilon_1 - \varepsilon_2)(\varepsilon_1 - \varepsilon_3)(\varepsilon_2 - \varepsilon_4)(\varepsilon_3 - \varepsilon_4), \\
D_{22} &= 2(\varepsilon_1^2 - \varepsilon_2\varepsilon_3)(\varepsilon_2\varepsilon_3 - \varepsilon_4^2) - 2\varepsilon_1(\varepsilon_2 - \varepsilon_3)^2\varepsilon_4, \\
D_{02} &= -2(\varepsilon_1^2 + \varepsilon_2\varepsilon_3)(\varepsilon_2\varepsilon_3 + \varepsilon_4^2) + 2\varepsilon_1(\varepsilon_2 + \varepsilon_3)^2\varepsilon_4, \\
D_{00} &= -2(\varepsilon_1^2 - \varepsilon_2\varepsilon_3)(\varepsilon_2\varepsilon_3 - \varepsilon_4^2) - 2\varepsilon_1(\varepsilon_2 + \varepsilon_3)^2\varepsilon_4 - 8\varepsilon_1\varepsilon_2\varepsilon_3\varepsilon_4.
\end{aligned} \tag{13}$$

For $s_3(\lambda)$, i.e. vertical polarization, N is computed from

$$\begin{aligned}
N_{14} &= -(\varepsilon_1 - \varepsilon_2)(\varepsilon_1 - \varepsilon_3)(\varepsilon_2 - \varepsilon_4)\varepsilon_3, \\
N_{34} &= (\varepsilon_1 - \varepsilon_2)(\varepsilon_1 - \varepsilon_3)(\varepsilon_2 - \varepsilon_4)\varepsilon_4, \\
N_{32} &= (\varepsilon_1 + \varepsilon_2)(\varepsilon_1 - \varepsilon_3)(\varepsilon_2 + \varepsilon_4)\varepsilon_4, \\
N_{1-2} &= (\varepsilon_1 + \varepsilon_2)(\varepsilon_1 + \varepsilon_3)(\varepsilon_2 - \varepsilon_4)\varepsilon_3, \\
N_{12} &= 2(\varepsilon_1^2\varepsilon_4^2 + \varepsilon_2^2\varepsilon_3^2) + (\varepsilon_3 + \varepsilon_4)[\varepsilon_1^2(\varepsilon_4 - \varepsilon_2) + \varepsilon_2^2(\varepsilon_3 - \varepsilon_1) + (\varepsilon_1 + \varepsilon_2)\varepsilon_3\varepsilon_4] \\
&\quad - \varepsilon_1\varepsilon_2(\varepsilon_3^2 + 6\varepsilon_3\varepsilon_4 + \varepsilon_4^2).
\end{aligned} \tag{14}$$

There exists a simple symmetry between $s_3(\lambda)$ and $c_3(\lambda)$ and thereby also $\alpha^{(v)}$ and $\alpha^{(h)}$: By substituting ε_i with $1/\varepsilon_i$ for all i $s_3(\lambda)$ transforms into $-c_3(\lambda)$ and vice versa. In the following,

we will therefore mainly focus on vertical polarization, because the corresponding results for horizontal polarization can be obtained by performing simple substitutions.

The general expression for $s_3(\lambda)$ simplifies substantially for simpler geometries. For a cut cylinder in a homogenous surrounding ($\varepsilon_1 \equiv \varepsilon$ and $\varepsilon_2 = \varepsilon_3 = \varepsilon_4 \equiv \varepsilon_h$) $s_3(\lambda)$, for example, reduces to

$$s_3(\lambda) = \frac{N_{12}(C_{12} - C_{10}) + N_{32}(C_{32} - C_{10})}{D_{00} + D_{20}C_{20} + D_{02}C_{02}} \frac{2}{S_{10}}, \quad (15)$$

where $D_{00} = -4\varepsilon\varepsilon_h$, $D_{20} = (\varepsilon + \varepsilon_h)^2$, $D_{02} = -(\varepsilon - \varepsilon_h)^2$, $N_{12} = (\varepsilon - 3\varepsilon_h)(\varepsilon - \varepsilon_h)/2$, and $N_{32} = (\varepsilon + \varepsilon_h)(\varepsilon - \varepsilon_h)/2$.

For $w \rightarrow 0$ the geometry describes a full cylinder lying on a substrate. In this case, the dominant contributions to the integrals of Eq. (7) are from $\lambda \gg 1$ and we are therefore allowed to approximate as $C_{11} \approx S_{11} \approx \exp[\lambda(\pi - w)]/2$ and $C_{10} \approx S_{10} \approx \exp(\lambda\pi)/2$. Using this and taking $\varepsilon_2 = \varepsilon_4$ we find

$$s_3(\lambda) \approx \frac{2(\varepsilon_1 - \varepsilon_3)\varepsilon_4 e^{-\lambda(2\pi+w)} [e^{2\lambda\pi}(\varepsilon_1 + \varepsilon_4) - 2(e^{2\lambda w} - 1)(\varepsilon_1 - \varepsilon_3)]}{(\varepsilon_1 + \varepsilon_4)[\varepsilon_3(\varepsilon_1 + \varepsilon_4) \cosh(\lambda w) + (\varepsilon_3^2 + \varepsilon_1\varepsilon_4) \sinh(\lambda w)]}, \quad (16)$$

which for $\lambda \gg 1$ can be approximated as

$$s_3(\lambda) \approx \frac{2(\varepsilon_1 - \varepsilon_3)\varepsilon_4 e^{-\lambda w}}{\varepsilon_3(\varepsilon_1 + \varepsilon_4) \cosh(\lambda w) + (\varepsilon_3^2 + \varepsilon_1\varepsilon_4) \sinh(\lambda w)}. \quad (17)$$

By performing the integral of Eq. (7) using the above expression for $s_3(\lambda)$ we obtain the simple result for the vertical polarizability

$$\alpha^{(v)} = \frac{4\pi\varepsilon_4}{w^2(\varepsilon_4 - \varepsilon_3)} \text{Li}_2 \left[\frac{(\varepsilon_3 - \varepsilon_1)(\varepsilon_3 - \varepsilon_4)}{(\varepsilon_3 + \varepsilon_1)(\varepsilon_3 + \varepsilon_4)} \right], \quad (18)$$

where $\text{Li}_s(z)$ is the polylogarithm (or Jonquire's function [36]). A resonance at $\varepsilon_1 = -\varepsilon_3$ is revealed. Note that, as expected, the polarizability is proportional to the radius squared $r^2 = 1/\sin^2 w \approx 1/w^2$ for w small. By performing similar approximations for the horizontally polarized case $c_3(\lambda)$ can be found as

$$c_3(\lambda) \approx \frac{2(\varepsilon_1 - \varepsilon_3)\varepsilon_3 \exp(-\lambda w)}{(\varepsilon_1 + \varepsilon_4)\varepsilon_3 \cosh(\lambda w) + (\varepsilon_3^2 + \varepsilon_1\varepsilon_4) \sinh(\lambda w)}, \quad (19)$$

which integrates to

$$\alpha^{(h)} = \frac{4\pi\varepsilon_3}{w^2(\varepsilon_4 - \varepsilon_3)} \text{Li}_2 \left[\frac{(\varepsilon_3 - \varepsilon_1)(\varepsilon_3 - \varepsilon_4)}{(\varepsilon_3 + \varepsilon_1)(\varepsilon_3 + \varepsilon_4)} \right]. \quad (20)$$

Again a resonance at $\varepsilon_1 = -\varepsilon_3$ is revealed. It should be noted that because of the approximations utilized $C_{11} \approx S_{11} \approx \exp[\lambda(\pi - w)]/2$ and $C_{10} \approx S_{10} \approx \exp(\lambda\pi)/2$ the substitutional symmetry between $s_3(\lambda)$ and $c_3(\lambda)$ has disappeared. Eq. (19) cannot be obtained from Eq. (17) by utilizing the simple symmetry stated above. Our results show that, for a cylinder lying on a surface, it is the dielectric constant of the medium above the surface that dictates the resonances of the polarizability. In fact, the resonance condition $\varepsilon_1 = -\varepsilon_3$ is identical to that of a cylinder in a homogenous ε_3 surrounding. However, the scaling of the polarizability for the two polarizations are different. For vertical resonances it scales with ε_4 whereas for horizontal resonances it scales with ε_3 .

By Taylor expanding the general expression for $s_3(\lambda)$ [Eqs. (12), (14), and (15)] for λ small we find

$$s_3(\lambda) \approx \frac{2}{\lambda} \left[-\frac{1}{\pi} + \frac{\varepsilon_3^{-1} + \varepsilon_4^{-1}}{(\varepsilon_1^{-1} + \varepsilon_4^{-1})(\pi - w) + (\varepsilon_2^{-1} + \varepsilon_3^{-1})w} \right]. \quad (21)$$

From this expansion it can be seen that $s_3(\lambda)$, and therefore also $\alpha^{(v)}$, has a resonance at the condition

$$(\varepsilon_1^{-1} + \varepsilon_4^{-1})(\pi - w) + (\varepsilon_2^{-1} + \varepsilon_3^{-1})w = 0. \quad (22)$$

Note the dependence on w of the resonance condition. For horizontal polarization the resonance condition can be obtained by utilizing the simple symmetry $\varepsilon_i \rightarrow 1/\varepsilon_i$. This yields

$$(\varepsilon_1 + \varepsilon_4)(\pi - w) + (\varepsilon_2 + \varepsilon_3)w = 0. \quad (23)$$

In the general case, for an arbitrary w , the integrals of Eq. (7) cannot be performed analytically. It is only possible in a few special cases. For a half-buried cylinder $w = \pi/2$ the results are presented in Ref. [33], but e.g. also for $w = 2\pi/3$, corresponding to a 3/4 buried cylinder, an analytical result can be obtained. We will not present these rather comprehensive calculations here, but instead note that when the analytical expressions of $s_3(\lambda)$ and $c_3(\lambda)$ are given, the integrals of Eq. (7) are straightforward to evaluate using numerical integration. There are no problems with convergence or singularities. In fact, if the integrals over λ are taken from 0 to 10 a fully converged result is obtained, except if w is very small.

3. Results

First, we present calculations of the polarizability of three different configurations using the approach outlined in Sec. 2. We consider (a) a cut cylinder in a homogenous surrounding ($\varepsilon_1 = \varepsilon$ and $\varepsilon_2 = \varepsilon_3 = \varepsilon_4 = \varepsilon_h = 1$), (b) a cut cylinder on a quartz surface ($\varepsilon_1 = \varepsilon$, $\varepsilon_2 = \varepsilon_4 = \varepsilon_h = 2.25$, and $\varepsilon_3 = 1$), and (c) a full cylinder partly buried in a quartz substrate ($\varepsilon_1 = \varepsilon_2 = \varepsilon$, $\varepsilon_4 = 2.25$, and $\varepsilon_3 = 1$). In order to identify the resonances, we consider metal-like cylinders with complex dielectric constants that have negative real parts and a small imaginary part. The small imaginary part has been added to prevent singularities at the resonances of the polarizability. Thus, the dielectric constant of the cylinder is in the following calculations given by $\varepsilon = \varepsilon_r + 0.01i$, where ε_r is negative. The result for configuration (a) is presented in Fig. 3. The figures to the left display the real (top) and imaginary (bottom) part of the vertical polarizability. The figures to the right display the same, but for the horizontal polarizability. Three different w 's are considered: $w = \pi/3$ corresponding to a 3/4 cylinder, $w = \pi/2$ a half cylinder, and $w = 2\pi/3$ a 1/4 cylinder. For configuration (a) Eqs. (22) and (23) give the following resonance conditions (for vertical and horizontal polarization, respectively)

$$\varepsilon = -\varepsilon_h \frac{\pi - w}{\pi + w} \quad \text{and} \quad \varepsilon = -\varepsilon_h \frac{\pi + w}{\pi - w}. \quad (24)$$

For vertical polarization the three different w 's considered give resonances at $\varepsilon_r = -1/2$, $-1/3$, and $-1/5$, and for horizontal polarization we find resonances at $\varepsilon_r = -2$, -3 , and -5 . All these resonances are clearly seen both in the real and the imaginary part of the polarizability (Fig. 3). For w small a resonance at $\varepsilon_r = -\varepsilon_h = -1$ is also expected [c.f. Eqs. (18) and (20)]. For $w = \pi/3$ this resonance is visible in the polarizability of both polarizations (Fig. 3). From Fig. 3 it can be seen that the resonance in the vertical polarizability moves towards larger ε_r for an increasing angle w , whereas the resonance in the horizontal polarizability moves towards smaller ε_r . For

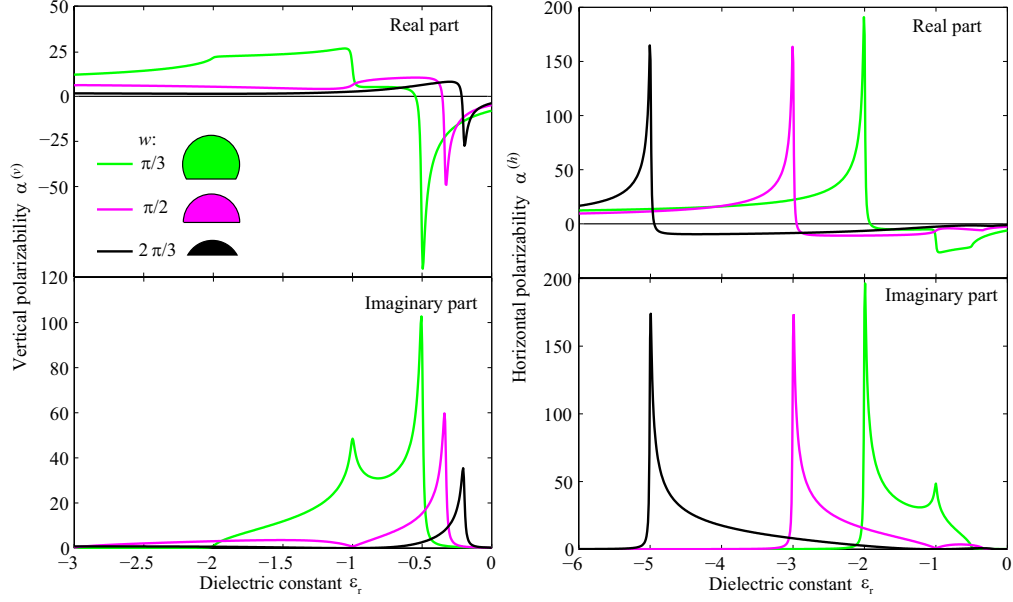


Fig. 3. Polarizability as a function of ϵ_r for three differently cut cylinders.

ordinary plasmonic metals like silver and gold this corresponds to a blue-shift of the resonance in the vertical polarizability and a red-shift in the horizontal. From the presented results it is clear that it is the geometry of the nanowire that dictates the location of the resonance. In fact it is the ratio between the size of the nanowire along the induced dipole moment to the size of the nanowire perpendicular to the induced dipole moment that is important. Thus, for the vertical polarizability it is the height to the width ratio, which is slowly decreasing for an increasing w that accounts for the small blue-shift of the resonance. For the horizontal polarizability it is the width to the height ratio, which is strongly increasing with larger w that accounts for the large red-shift of the resonance.

For a cut cylinder on a surface, configuration (b), the calculated polarizability is depicted in Fig. 4. For this configuration the resonance conditions from Eqs. (22) and (23) give

$$\epsilon = -\epsilon_h \epsilon_3 \frac{\pi - w}{\epsilon_3 \pi + \epsilon_h w} \quad \text{and} \quad \epsilon = -\frac{\epsilon_h \pi + \epsilon_3 w}{\pi - w}. \quad (25)$$

For the three w 's and vertical polarization this yields $\epsilon_r \approx -0.86, -0.53$, and $\epsilon_r = -0.3$. For horizontal polarization we expect resonances at $\epsilon_r = -3.875, -5.5$, and -8.75 . These resonances are all clearly seen in the calculated polarizability (Fig. 4). For configuration (b) the resonance at $\epsilon = -\epsilon_3 = -1$, which is expected for w small [c.f. Eqs. (18) and (20)], is largely visible in both the vertical and horizontal polarizability for $w = \pi/3$. Again it can be seen how the resonance in the vertical (horizontal) polarizability blue- (red)-shifts when the angle w increases. As described above, this is due to the changing geometry of the nanowire when w increases. By comparing Fig. 4 to Fig. 3 it can be seen that all the resonances (except for the one fixed at $\epsilon_r = -1$ in the $w = \pi/3$ configuration) are red-shifted. This is because the effective surrounding index that the nanowire feels in the geometry of Fig. 4 is larger than in the geometry of Fig. 3. However, it should be noted that the relative shift of the resonances is very similar in the two configurations.

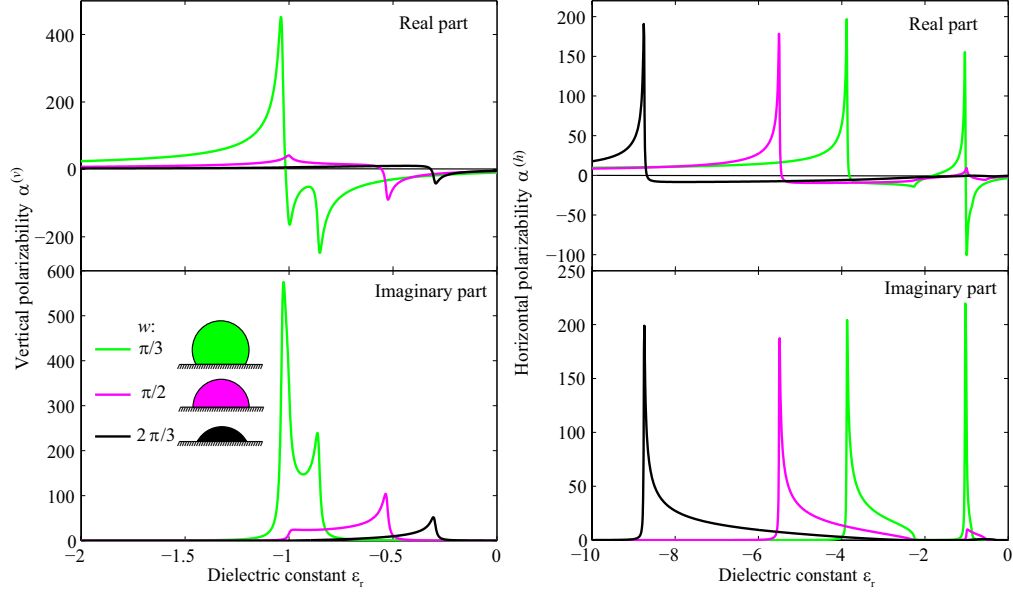


Fig. 4. Polarizability as a function of ϵ_r for three differently cut cylinders on a quartz surface.

The polarizability of configuration (c), a partly buried full cylinder, is presented in Fig. 5. In this case, Eqs. (22) and (23) yield

$$\epsilon = -\frac{\pi\epsilon_3\epsilon_4}{\epsilon_3(\pi-w) + \epsilon_4w} \quad \text{and} \quad \epsilon = -\frac{\epsilon_4(\pi-w) + \epsilon_3w}{\pi}. \quad (26)$$

Thus, for the three w 's considered, we expect resonances at $\epsilon_r \approx -1.59$, -1.38 , and -1.23 and $\epsilon_r \approx -1.83$, -1.63 , and -1.42 for vertical and horizontal polarization, respectively. All these resonances are clearly seen in the polarizability (Fig. 5). However, the figure reveals that three different resonances come into play: The one determined by Eq. (26), and two others fixed at $\epsilon_r = -\epsilon_3 = -1$ and $\epsilon_r = -\epsilon_h = -2.25$. The latter two are identical to the resonances of a full cylinder in a homogenous surrounding described by dielectric constants $\epsilon_h = 1$ and $\epsilon_h = 2.25$, respectively. It is clear from the results that the $\epsilon_r = -1$ resonance is strongest when w is small, i.e. when a large part of the cylinder is in the medium 3, whereas the $\epsilon_r = -2.25$ resonance is strongest for w large, i.e. when the cylinder is largely buried in the substrate. These observations agree nicely with the theory for w very small, which predicts a resonance at $\epsilon_1 = -\epsilon_3 = -1$, see Eqs. (18) and (20). From the results, in particular the imaginary part of the polarizability, it can also be seen how the effective index of the surrounding medium controls the cutoff between absorption in the blue and the red part of the dielectric spectrum. The full range of absorption is restricted to the dielectric range $\epsilon_r \in [-2.25, -1]$ with a gap separating the blue and the red parts. The cutoff controlling the position of this gap clearly reflects the degree of burial of the nanowire. Thus, when most of the nanowire is in air, significant absorption in the blue part of the spectrum is observed. However, as the nanowire moves into the substrate, the large absorption shifts towards the red part of the spectrum. The main results of the three configurations are summarized in Table 1.

Lastly, we have calculated the polarizability in the case of $w \rightarrow 0$ taking $\epsilon_2 = \epsilon_4 = \epsilon_h$, i.e. the limit where the geometry resembles a full cylinder lying on a surface. This allows us to use the

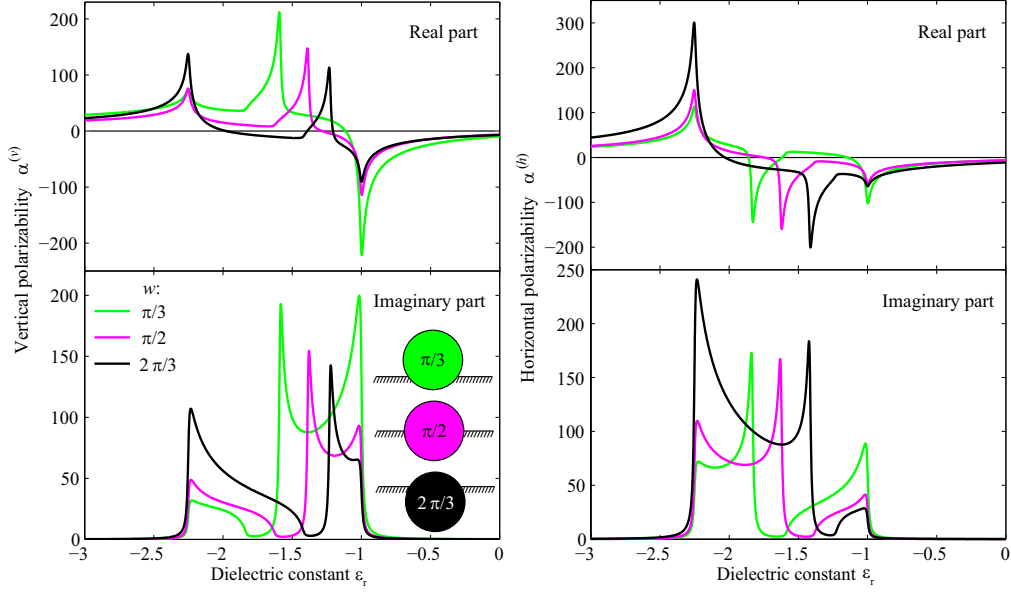


Fig. 5. Polarizability as a function of ϵ_r for three cylinders differently buried in a quartz surface.

Table 1. Summary of the resonance conditions for the nanowire dielectric constant of the three configurations (a), (b), and (c) investigated.

Configuration	$w = \pi/3$	$w = \pi/2$	$w = 2\pi/3$	Resonance condition
(a) vertical	$-1/2$	$-1/3$	$-1/5$	$-\epsilon_h(\pi - w)/(\pi + w)$
(a) horizontal	-2	-3	-5	$-\epsilon_h(\pi + w)/(\pi - w)$
(b) vertical	-0.86	-0.53	-0.30	$-\epsilon_h\epsilon_3(\pi - w)/(\epsilon_3\pi + \epsilon_h w)$
(b) horizontal	-3.88	-5.50	-8.75	$-(\epsilon_h\pi + \epsilon_3 w)/(\pi - w)$
(c) vertical	-1.59	-1.38	-1.23	$-(\pi\epsilon_3\epsilon_4)/[\epsilon_3(\pi - w) + \epsilon_4 w]$
(c) horizontal	-1.83	-1.63	-1.42	$-\epsilon_4(\pi - w) + \epsilon_3 w]/\pi$

approximate analytical expressions of Eqs. (18) and (20) to calculate the polarizability. First, we consider a cylinder with a metal-like dielectric constant $\epsilon = \epsilon_r + 0.01i$, where ϵ_r is negative. For $\epsilon_3 = 1$ and three different substrates $\epsilon_h = 2.25$ (quartz), 5 (silicon nitride), and 11.9 (silicon), the imaginary part of the horizontal polarizability is displayed in Fig. 6 (a). Because the polarizabilities for the two polarizations in this configuration, except for a scaling, are identical, we only present results for the horizontal polarizability. The results show that the imaginary part of the polarizability rises at the resonance $\epsilon_r = -1$ and vanishes again for $\epsilon_r < -\epsilon_h$. This is clearly seen from the zoom [inset of Fig. 6 (a)]. Thus, by choosing a substrate with a large dielectric constant, absorption of light in the nanowire is sustained over a relatively broad range of wavelengths. This is more clearly seen in Fig. 6 (b), where we have calculated the imaginary part of the horizontal polarizability versus the photon energy of a silver nanowire on different substrates using a dielectric constant for silver taken from the experiments of Johnson and Christy [37]. Note how the low-frequency tail of the resonance broadens as the dielectric constant of the substrate increases. On the high-frequency side of the resonance the effect of interband absorption in the silver is seen. Lastly it should be noted, that nanocylinders on surfaces

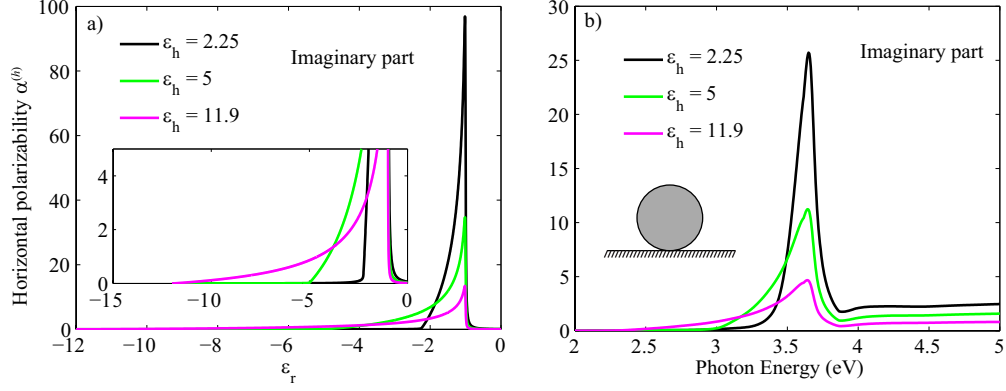


Fig. 6. Imaginary part of the horizontal polarizability for a full cylinder lying on three different surfaces. (a) versus ϵ_r and (b) versus the photon energy. In (a), we use $\epsilon = \epsilon_r + 0.01i$ and in (b) we use a dielectric constant for silver taken from the experiments of Ref. [37].

have been analyzed before using numerical analysis [38] and more recently transformation optics [39]. Compared to the full approaches of Refs. [38, 39] the approximate polarizabilities of Eqs. (18) and (20) are easy to evaluate in that they only involve the calculation of a single polylogarithm.

4. Conclusion

The electrostatic polarizability of a general geometry consisting of two nanowire segments forming a cylinder that can be arbitrarily buried in a substrate is derived in a semi-analytical approach using bipolar coordinates, cosine-, and sine-transformations. From the derived expressions we have calculated the polarizability of four important metal nanowire geometries: (1) a cut cylinder in a homogenous surrounding, (2) a cut cylinder on a surface, (3) a full cylinder partly buried in a substrate, and (4) a cylinder lying on a surface. Our results give physical insight into the interplay between the multiple resonances of the polarizability of metal nanowire geometries at surfaces, and provide an exact, fast, and easy scheme for optimizing metal nanowire structures for various applications within plasmonics.

Acknowledgments

The authors gratefully acknowledge support from the project “Localized-surface plasmons and silicon thin-film solar cells - PLATOS” financed by the Villum foundation.